Supporting Information

Assessing the Perturbing Effects of Drugs on Lipid Bilayers using Gramicidin Channel-Based *in Silico* and *in Vitro* Assays

Delin Sun[1], Thasin A. Peyear[2], W. F. Drew Bennett[1], Matthew Holcomb[1], Stewart He[1], Fangqiang Zhu[1], Felice C. Lightstone[1], Olaf S. Andersen[2] and Helgi I. Ingólfsson[1]

[1]Biosciences and Biotechnology Division, Physical and Life Sciences Directorate, Lawrence Livermore National Laboratory, Livermore, CA 94550.

[2]Department of Physiology and Biophysics, Weill Cornell Medicine, New York, NY 1006.

Contents:

Supplementary Methods

Development of Coarse-Grained Model for gA. The major component of the naturally occurring gramicidin mixture is gA, with the amino acid sequence of formyl-*L*-Val[1]-*D*-Gly[2]-*L*-Ala[3]-*D*-Leu[4]-*L*-Ala[5]-*D*-Val[6]-*L*-Val[7]-*D*-Val[8]-*L*-Trp[9]-*D*-Leu[10]-*L*-Trp[11]-*D*-Leu[12]-*L*-Trp[13]-*D*-Leu[14]-*L*-Trp[15]-ethanolamine. The gA peptide has alternating *L*- and *D*-amino acids, and the peptide sequence is capped by a formyl group at the N-terminus and an ethanolamine group at the C-terminus. These features make the gA peptide fold into a $\beta^{6.3}$-helical conformation in lipid bilayers, with the Trp-rich C-terminal bound at the lipid bilayer/water interface and the formyl-N-terminus pointing toward the bilayer center. Two gA subunits can dimerize to form a channel that is stabilized by a maximum of six hydrogen bonds between the 1Val[1]-2Ala[5], 1Ala[3]-2Ala[3] and 1Ala[5]-2Val[1] amino acid pairs. The hydrogen bond interactions are strong, with each hydrogen bond contributing ~4 kcal/mol toward the channel's stability.[1-2]

Our coarse-grained (CG) model for the $\beta^{6.3}$-helical gA monomer is based on the Martini force field (version 2.2),[3-4] which models intermolecular interactions with tabulated parameters (C_{ij}^{6} and C_{ij}^{12}) for the Lennar-Jones (LJ) potential, $V_{LJ}(r_{ij}) = C_{ij}^{(12)}/r_{ij}^{12} - C_{ij}^{(6)}/r_{ij}^{6}$. The CG structure for the gA channel (Fig. S1 (a)), was obtained from the equilibrated all-atom (AA) gA dimer structure from our previous work[5] using the *martinize* script. The $\beta^{6.3}$-helical conformation was maintained with an elastic network (part of the Martini protein force field)[4] with an elastic bond force constant of 500 $kJ{\cdot}mol^{-1}{\cdot}nm^{-2}$. The CG backbone polarity/bead types were adjusted to fit the alternating *L*- and *D*-amino acid $\beta^{6.3}$-helical secondary structure based on the number of h-bonds between the corresponding AA residues. The formyl group (FOR) at the N-terminus and the ethanolamine (ETA) at the C-terminus of gA were modeled with a single SN0 and P2 CG bead type, respectively. The strength of the hydrogen bonds between two gA monomers is underestimated when using the Martini force field and the standard bead type mapping,[3] and thus the gA dimer quickly dissociated in the thick $DC_{22:1}PC$ lipid bilayer (see Fig. S2 (a)). We therefore developed a new bead type (gAb) for the formyl, Val[1], Gly[2], Ala[3], Leu[4] and Ala[5] backbone beads, where the hydrogen bond interactions between the N-termini were incorporated through strong gAb-gAb bead attractions. Similarly, a new bead type (gAd) was created for the Leu[12], Leu[14] and ethanolamine backbone beads to model the interactions between the gA C-terminus and the lipid phosphate (Qa bead), glycerol groups (Na bead). The LJ parameters for the interactions between the gAb-gAb, gAd-Qa and gAd-Na pairs were tuned to capture the potential of mean force (PMF) for gA channel dissociation as determined from the AA replica-exchange umbrella sampling (REUS) simulations (Fig. 1 (a) in main text). This optimization resulted in the gAb-gAb bead interactions with LJ parameters of $C_{ij}^{6} = 0.31\ kJ \cdot mol^{-1} \cdot nm^{6}$ and $C_{ij}^{12} = 0.0036\ kJ \cdot mol^{-1} \cdot nm^{12}$, gAd-Qa and gAd-Na interactions with LJ parameters of $C_{ij}^{6} = 0.32\ kJ \cdot mol^{-1} \cdot nm^{6}$ and $C_{ij}^{12} = 0.0037\ kJ \cdot mol^{-1} \cdot nm^{12}$, respectively.

The chemical structures for capsaicin, resveratrol, octanol, C12E6, Triton X-100, FC12, cyclohexane and cholesterol and the corresponding CG schemes for the eight drug-like small molecules are shown in Fig. S1 (b). The Martini topology files for the eight small molecules are from previous work.[3, 6-8]

Unbiased Coarse-Grained MD Simulations. The v-scale thermostat[9] and Berendsen barostat[10] were used to control the system's temperature and pressure. The standard Martini parameters, called new-rf[11] were used, with the cut-off distance for LJ interactions and short-range electrostatics at 1.1 nm. A relative dielectric constant of 15 was used to screen electrostatic interactions between ions and lipid heads. The time step was 20 fs.

The unbiased CG simulations were used to validate the CG gA model by investigating the structural stability of the gA channel in the thick $DC_{22:1}PC$ bilayer. Fig. S2 (a) shows the time series for the center-of-mass (COM) distance between the two gA monomers in the channel structure. It is found that two gA monomers remain associated with the developed CG gA model. The average COM distance between the monomers in the CG model is 1.34 ± 0.03 nm, indistinguishable from AA simulation result, 1.33±0.01 nm. Fig. S2 (b) shows the root-mean-squared displacement (RMSD) of the gA channel. The RMSD profiles from the CG simulations tends to fluctuate, much more than the AA simulation results. This is caused by the wobbling of the two gA monomers (Fig. S2 (c)) in the CG simulations, which is not observed in the AA MD simulations.

Unbiased CG MD simulations were also run to investigate the drugs' effects on the bilayer's hydrophobic thickness. This was done by removing the gA channel from the 18 systems followed by 2 μs CG MD simulation. During the 2 μs MD simulations, only octanol was found to frequently transfer between the bilayer and the water phases.

PMF Profile Decomposition. Using the force integration approach, it is theoretically possible to decompose the PMF into different energetic contributions.[12-13] The four energetic components can be evaluated by

$$\Delta G_{gA-X}^{M\leftrightarrow D} = -\int_{dM}^{dD} \langle F_{\xi}^{gA-X} \rangle_{\xi} \, d\xi, \tag{S1}$$

where $\langle F_{\xi}^{gA-X} \rangle_{\xi}$ is the mean force between one gA monomer and component X (where X may be the second gA monomer, lipids in the bilayer, solvent, or the drugs) projected along the gA-gA center-of-mass distance reaction coordinate (ξ); *dM* and *dD* are the gA-gA center-of-mass distances for the monomer and dimer states. To calculate the interacting force between the center-of-mass of one gA monomer and the center-of-mass of group X (X = lipid bilayer, gA, drugs or solvent), we first extracted the coordinates for gA+X only from the CG-REUS simulation trajectories with the GROMACS *trjconv*

utility. The center-of-mass interacting force was obtained the with GROMACS *traj* utility. The obtained Cartesian forces were then projected onto the vector formed between the center-of-mass positions for the two gA monomers. The force decomposition was done for all 56 umbrella sampling windows for each simulation system, and the derived PMF profiles with such decomposed force integration (DFI) approach are plotted in Figs. S10 and S11. It should be noted, however, that the transformation from the three-dimensional Cartesian coordinates to the polar coordinate system produces a Jacobian correction term ($2k_BT\ ln(d)$) in the PMF.[14] Therefore, the DFI approach derived PMF profiles (Figs. S10 and S11) were corrected by including the Jacobian term.

All-Atom MD Simulations. All unbiased AA simulations were done in the semi-isotropic ensemble at 310.15 K and 1 bar using GROMACS 2018.[15] The Nosé-Hoover thermostat[16-17] and the Parrinello-Rahman barostat[18] were used to maintain temperature and pressure. The LINCS algorithm[19] was used to constrain water geometry and covalent bonds involving a hydrogen atom. Lennard-Jones interactions were switched off smoothly at 1-1.2 nm and the Particle Mesh Ewald method[20] was used to treat long-range electrostatics with a real space cutoff distance of 1.2 nm. Long-range dispersion corrections to the energy and pressure were not applied. Snapshots of each simulation were saved every 20 ps.

All of the CG and AA simulations were run on the *Lassen* supercomputer at Lawrence Livermore National Laboratory, and a summary of all the simulations is listed in Table S1.

Estimating the Changes in Bilayer Deformation Energy. The drug-induced changes in $R_{\mathrm{Drug}}/R_{\mathrm{Cntrl}}$ in the $DC_{22:1}PC$ LUVs, where the concentration of non-conducting gramicidin monomers ([M]) is much higher than the concentration of conducting gramicidin dimers ([D]), allow us to estimate $\Delta\Delta G^{M\leftrightarrow D}|_{Drug}$ as[5]:

$$\begin{aligned}\Delta\Delta G^{M\leftrightarrow D}|_{Drug} &= -k_BT\cdot ln\left\{\frac{K^{M\leftrightarrow D}_{Drug}}{K^{M\leftrightarrow D}_{Cntrl}}\right\} = -k_BT\cdot ln\left\{\frac{[D]_{Drug}/[M]^2_{Drug}}{[D]_{Cntrl}/[M]^2_{Cntrl}}\right\}\\ &\approx -k_BT\cdot ln\left\{\frac{[D]_{Drug}}{[D]_{Cntrl}}\right\} \approx -k_BT\cdot ln\left\{\frac{R_{Drug}}{R_{Cntrl}}\right\}\end{aligned} \tag{S2}$$

where k_B is Boltzmann's constant, T the temperature in kelvin, $K^{M\leftrightarrow D}$ the gramicidin monomer ↔ dimer equilibrium constant, and the subscripts "Cntrl" and Drug" indicate the absence and presence of drug. For comparison between the experimental and CG estimates, we note that $R_{\mathrm{Drug}}/R_{\mathrm{Cntrl}}$ increases as an approximately linear function of drug concentration,[21-22] and we used the results in Fig. S7 to estimate what $R_{\mathrm{Drug}}/R_{\mathrm{Cntrl}}$ would be at a drug:lipid ratio = 0.084, the ratio used in the CG simulations, and used this estimate for $R_{\mathrm{Drug}}/R_{\mathrm{Cntrl}}$ to calculate $\Delta\Delta G^{M\leftrightarrow D}|_{Drug}$.

To compare the experimental results with the CG simulation results, we fitted the $R_{\mathrm{Drug}}/R_{\mathrm{Cntrl}}$ vs. m_{Drug} relations with straight lines:[21]

$$R_{Drug}/R_{Cntrl} = 1 + \frac{m_{Drug}}{M_{Drug}} \tag{S3}$$

where M_{Drug} denotes the value of m_{Drug} at which $R_{\mathrm{Drug}}/R_{\mathrm{Cntrl}} = 2$, which also allowed us to determine the predicted values of $R_{\mathrm{Drug}}/R_{\mathrm{Cntrl}}$ when $m_{\mathrm{Drug}} = 0.084$. We then could estimate $\Delta\Delta G^{M\leftrightarrow D}|_{Drug}$ at $m_{\mathrm{Drug}} = 0.084$ as $-k_{\mathrm{B}}T \cdot \ln\left\{R_{\mathrm{Drug}} / R_{\mathrm{Cntrl}}\right\}$. Table S4 summarizes information about m_{Drug}, as well as the predicted values of $R_{\mathrm{Drug}}/R_{\mathrm{Cntrl}}$ and $\Delta\Delta G^{M\leftrightarrow D}|_{Drug}$ when $m_{\mathrm{Drug}} = 0.084$.

The cholesterol-induced $\Delta\Delta G^{M\leftrightarrow D}|_{Drug}$ values were estimated from the ratio of the gramicidin:lipid molar ratios that were needed to give approximately equal quench rates in cholesterol-free and cholesterol-containing LUVs (Fig. S6):

$$\begin{aligned}\Delta\Delta G^{M\leftrightarrow D}|_{Chol} &= -k_B T \cdot ln\left\{\frac{K^{M\leftrightarrow D}_{Chol}}{K^{M\leftrightarrow D}_{Cntrl}}\right\} = -k_B T \cdot ln\left\{\frac{[D]_{Chol}/[M]^2_{Chol}}{[D]_{Cntrl}/[M]^2_{Cntrl}}\right\} \\ &= -k_B T \cdot \left(ln\left\{\frac{[D]_{Chol}}{[D]_{Cntrl}}\right\} + ln\left\{\frac{[M]^2_{Cntrl}}{[M]^2_{Chol}}\right\}\right) \approx -k_B T \cdot ln\left\{\frac{[M]^2_{Cntrl}}{[M]^2_{Chol}}\right\} \\ &\approx -k_B T \cdot ln\left\{\frac{[T]^2_{Cntrl}}{[T]^2_{Chol}}\right\}\end{aligned} \tag{S4}$$

where [T] denotes the total concentration of gramicidin ([T] = [M] + 2·[D]), and [M] >> [D], such that [T] ≈ [M].

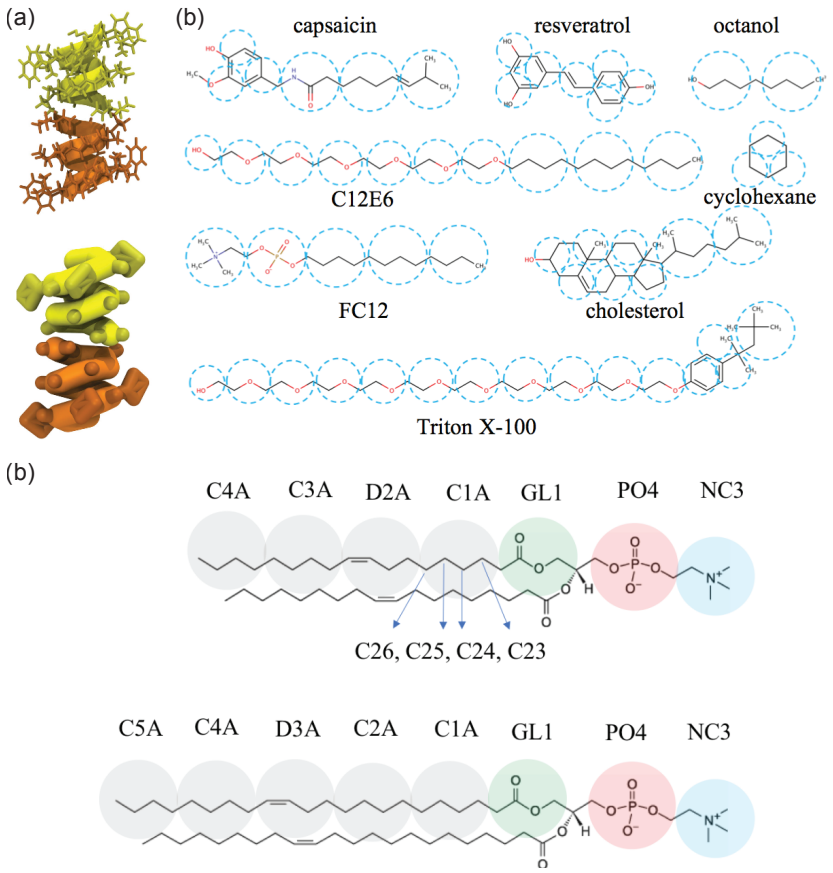

Figure S1. AA and CG models for the (a) gA channel, (b) the eight drug molecules, and (c) the two lipids: $DC_{18:1}PC$ and $DC_{22:1}PC$. The hydrophobic thickness of the lipid bilayer is calculated by averaging the trans-bilayer distance between the center-of-mass of all CA1 beads (for CG model) or the center-of-mass for C23, C24, C25, C26 atoms (for AA model) in the upper and lower leaflets.

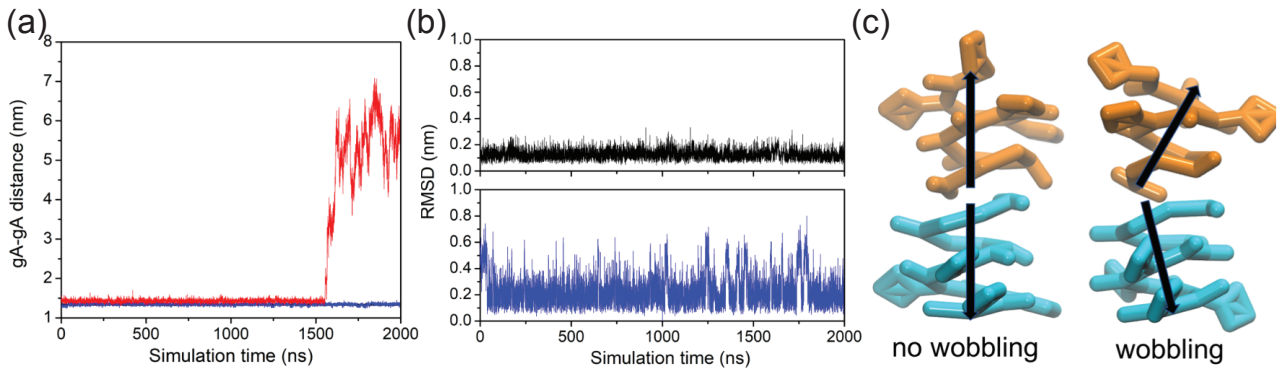

Figure S2. (a) Center-of-mass distance between two gA monomers in the gA channel embedded in the $DC_{22:1}PC$ bilayer predicted with the CHARMM36 model (black, underneath blue line), the Martini model without specific tuning of beads between the two gA monomers to represent the across monomer hydrogen bonds (red) and the Martini gA model with hydrogen bond tuning (blue). The profiles predicted with the AA and the tuned CG gA model almost overlap. (b) The root-mean-squared displacement of the gA channel predicted with CHARMM36 model (black) and the tuned Martini gA model (blue). The fluctuations in the CG RMSD profile are caused by the monomer-monomer wobbling in the CG simulations, as illustrated in (c).

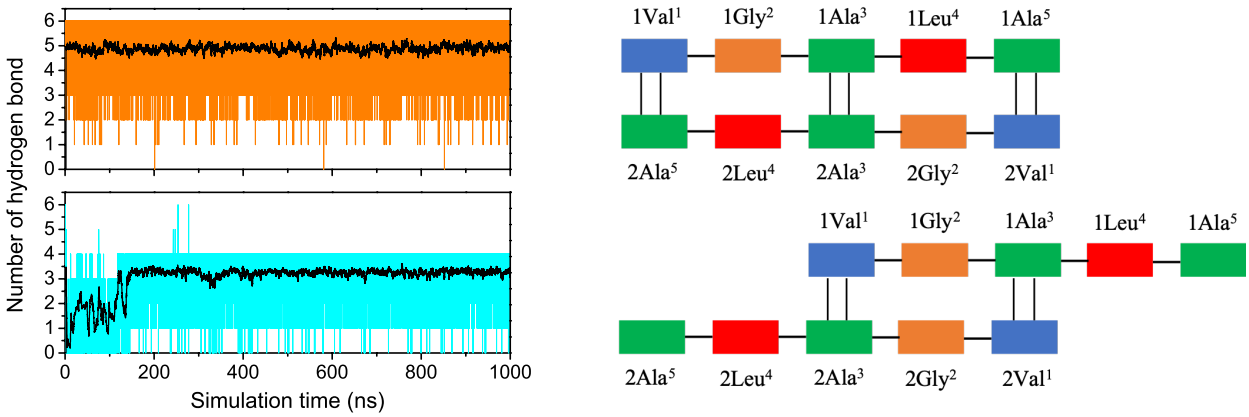

Figure S3. In the AA-REUS simulations, two structurally different channels are formed at the gA-gA distance of ~1.3 and ~1.5 nm. At the gA-gA distance of ~1.3 nm, the two monomers can form a maximum of six hydrogen bonds between the $1Val^{1}$-$2Ala^{5}$, $1Ala^{3}$-$2Ala^{3}$ and $1Ala^{5}$-$2Val^{1}$ amino acid pairs (orange line) while at the gA-gA distance of ~1.5 nm, only a maximum number of four hydrogen bonds can be formed between the $1Val^{1}$-$2Ala^{3}$ and $1Ala^{3}$-$2Val^{1}$ amino acid pairs (cyan line). The AA-REUS simulations reach equilibrium after 400 ns, where the running averaged numbers of hydrogen bond (black line) become stable.

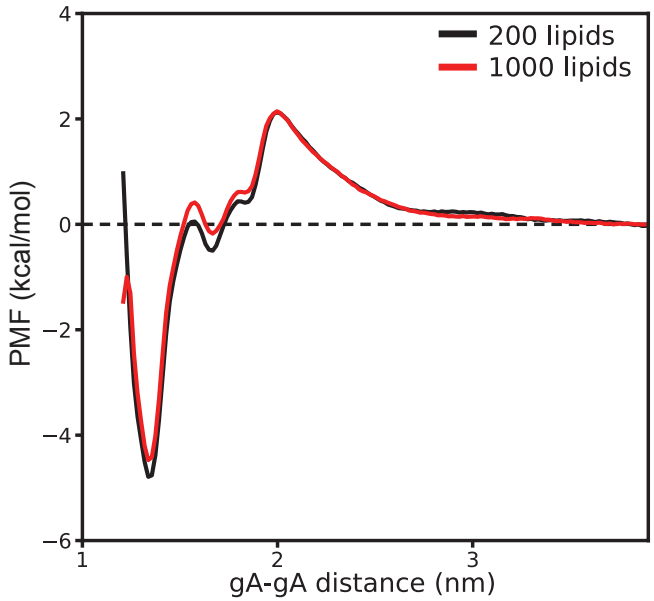

Figure S4. Effect of simulation system size on the PMF for gA monomer/dimer transition in $DC_{22:1}PC$ bilayers.

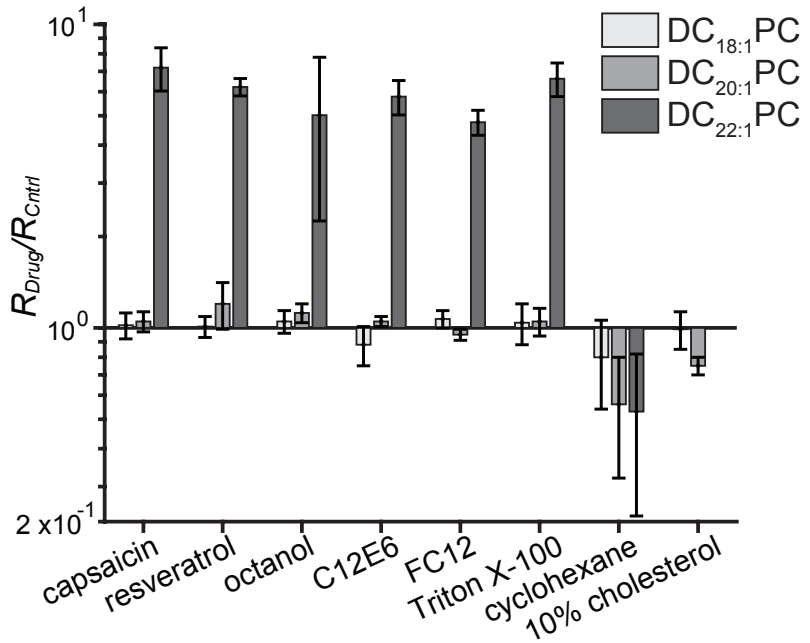

Figure S5. Effects of drugs on the fluorescence quench rates (gramicidin monomer ↔ dimer equilibrium) in $DC_{18:1}PC$, $DC_{20:1}PC$, and $DC_{22:1}PC$ LUVs doped with gD. The aqueous drug concentrations were 100, 30, 1800, 10, 300, 30, and 30,000 μM for capsaicin, resveratrol, octanol, C12E6, FC12, Triton X-100, and cyclohexane, respectively and the estimated molar ratios of the drugs in the bilayers were 0.32, 0.02, 0.48, 0.04, 0.21, 0.04, and 0.93, respectively; cholesterol was added at a molar ratio of cholesterol:lipid of 1:10 when preparing the LUVs. Mean ± S.D. n = 3-4

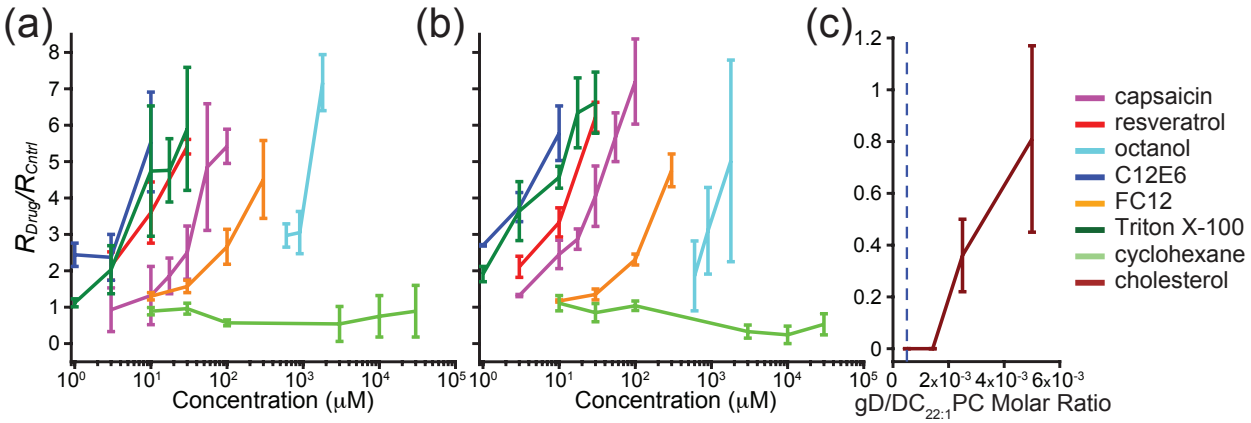

Figure S6. Dose-response curves for the tested drugs' effect on R_{Drug}/R_{Cntrl} in $DC_{22:1}PC$+gA and $DC_{22:1}PC$+gD bilayers. Results for the seven drugs that can be added through the aqueous phase in $DC_{22:1}PC$+gA (a) and $DC_{22:1}PC$+gD (b). The bilayer-modifying potency referenced to the aqueous solution decreases from left to right. (c) Shows results obtained in $DC_{22:1}PC$ cholesterol bilayers at a cholesterol:$DC_{22:1}PC$ of 1:9 (10% cholesterol in the membrane) as function of the gD:$DC_{22:1}PC$ ratio; the quench rates are normalized to the rates in cholesterol-free bilayers. There was no observable activity at the standard 1:2,000 gD:$DC_{22:1}PC$ ratio, there is at a gD:$DC_{22:1}PC$ ratio of 1:500, but R_{Drug}/R_{Cntrl} was only ≈ 1 at a gD:$DC_{22:1}PC$ ratio of 1:200, 10-fold higher than in the cholesterol-free membranes.

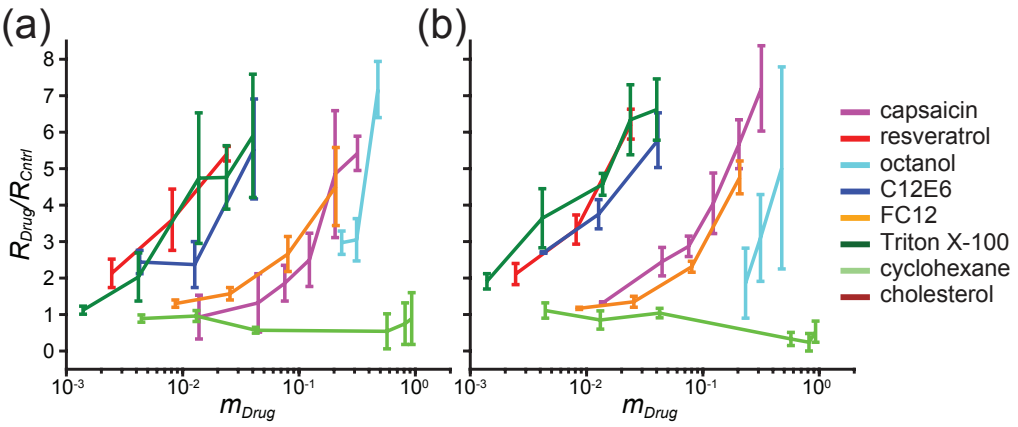

Figure S7. Dose-response curves for the tested drugs' effect on R_{Drug}/R_{Cntrl} in $DC_{22:1}PC$+gA (a) and $DC_{22:1}PC$+gD (b) bilayers based on the drugs' mole fractions in the bilayer; results for the seven drugs that can be added through the aqueous phase. The bilayer-modifying potency, referenced to the drugs' mole-fraction in the membrane, m_{Drug}, decreases from left to right.

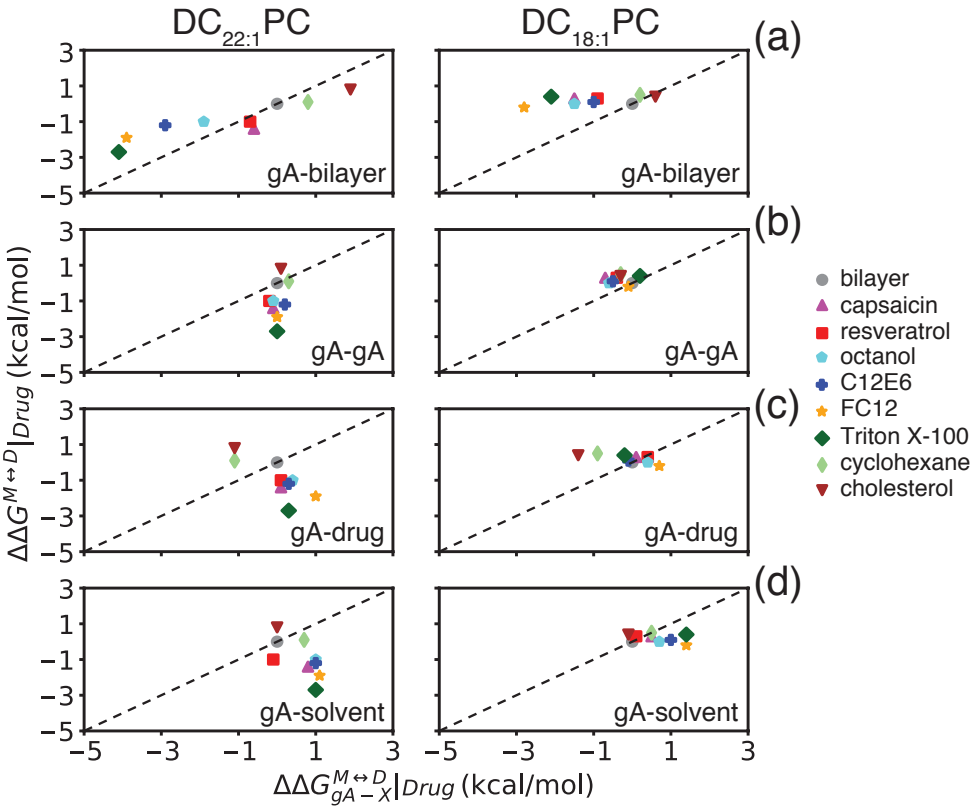

Figure S8. Correlation between the simulation derived $\Delta\Delta G^{M\leftrightarrow D}|_{Drug}$ and PMF decomposition derived $\Delta\Delta G^{M\leftrightarrow D}_{gA-X}$, where X represents lipid bilayer (a), gA (b), drug (c) and solvent (d). The $\Delta\Delta G^{M\leftrightarrow D}|_{Drug}$ values are well correlated with the $\Delta\Delta G^{M\leftrightarrow D}_{gA-bilayer}$ in the thick $DC_{22:1}PC$ bilayer whereas the correlation is poor in the thinner $DC_{18:1}PC$ bilayer.

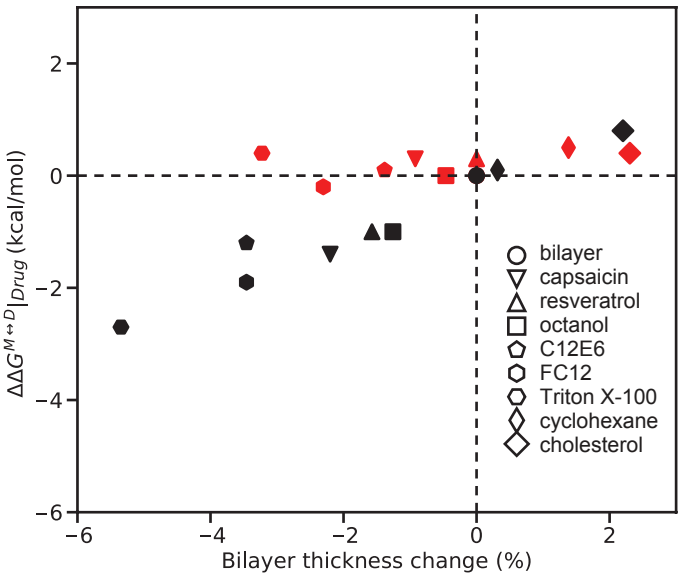

Figure S9. Correlation between the simulation derived $\Delta\Delta G^{M\leftrightarrow D}|_{Drug}$ and the drugs-induced bilayer thickness change in the $DC_{18:1}PC$ bilayer (red) and the $DC_{22:1}PC$ bilayer (black).

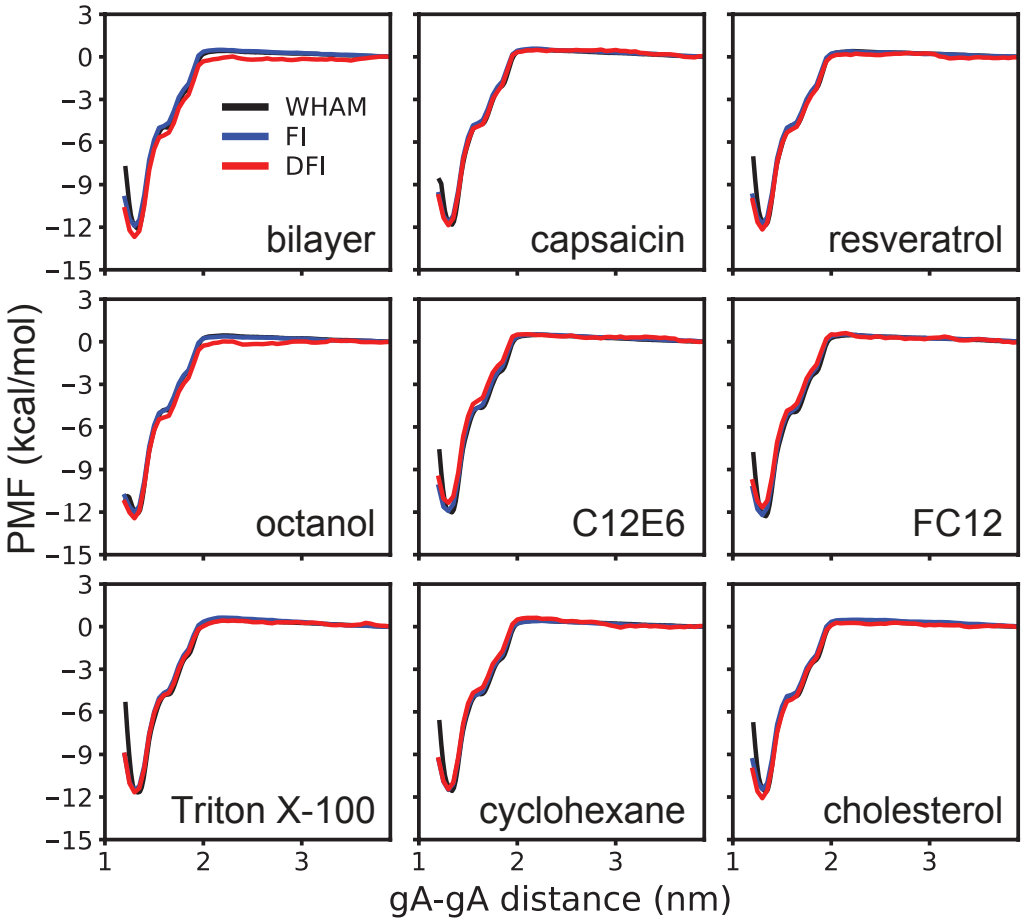

Figure S10. PMF for gA monomer ↔ dimer transition in the $DC_{18:1}PC$ derived with WHAM, force integration (FI) and decomposed force integration (DFI) approaches. Results for the eight different drugs as well as pure $DC_{18:1}PC$ bilayer are shown.

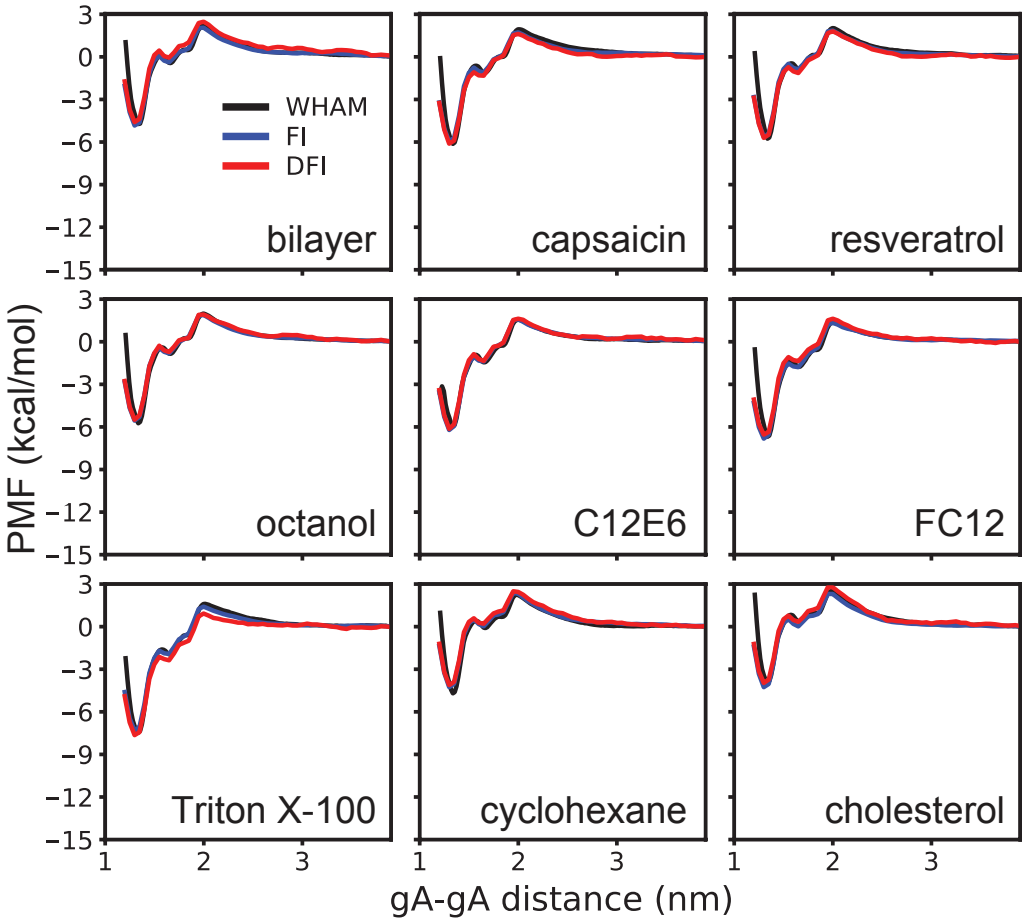

Figure S11. PMF for gA monomer ↔ dimer transition in the $DC_{22:1}PC$ derived with WHAM, FI and DFI approaches. Results for the eight different drugs as well as pure $DC_{22:1}PC$ bilayer are shown.

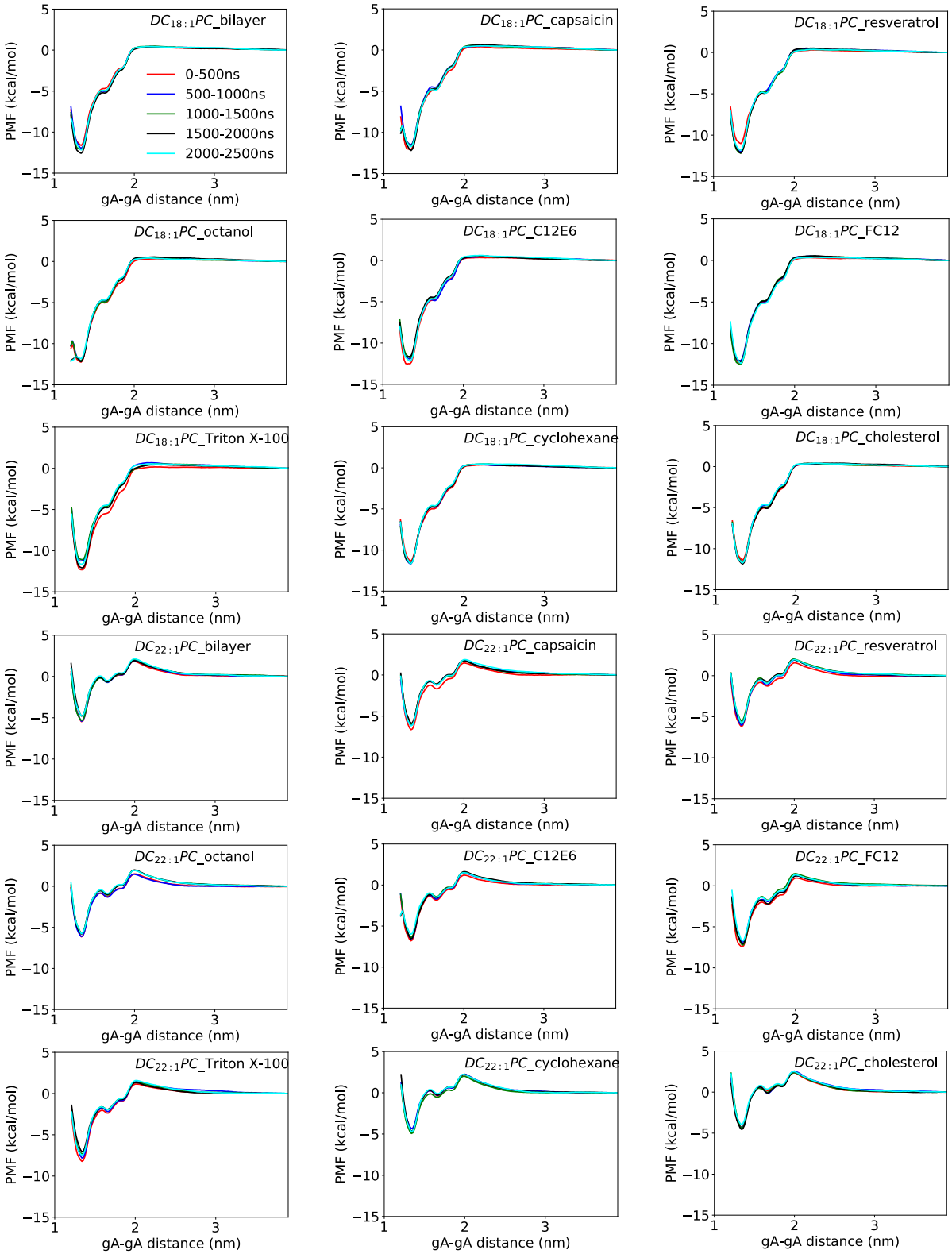

Figure S12. Convergence analysis of the CG PMF profiles. For each system, five independent PMF profiles were plotted using the 0-500 ns, 500-1000 ns, 1000-1500 ns and 1500-2000 ns data for each umbrella sampling window.

Table S1. Summary of all AA and CG MD simulations performed in this work. The unit for the simulation time is microsecond (μs).

Systems $DC_{18:1}PC$ with	Unbiased MD simulations		REUS simulations	
	AA	CG	AA	CG
bilayer only	0.5	2		
capsaicin	0.5	2		
resveratrol	0.5	2		
octanol	0.5	2		
C12E6	0.5	2		
FC12	0.5	2		
Triton X-100	0.5	2		
cyclohexane	0.5	2		
cholesterol	0.5	2		
gA	2	2	56	140
capsaicin+gA		2		140
resveratrol+gA		2		140
octanol+gA		2		140
C12E6+gA		2		140
FC12+gA		2		140
Triton X-100+gA		2		140
cyclohexane+gA		2		140
cholesterol+gA		2		140
Systems $DC_{22:1}PC$ with	Unbiased MD simulations		REUS simulations	
	AA	CG	AA	CG
bilayer only	0.5	2		
capsaicin	0.5	2		
resveratrol	0.5	2		
octanol	0.5	2		
C12E6	0.5	2		
FC12	0.5	2		
Triton X-100	0.5	2		
cyclohexane	0.5	2		

cholesterol	0.5	2		
gA	2	2	56	140
capsaicin+gA		2		140
resveratrol+gA		2		140
octanol+gA		2		140
C12E6+gA		2		140
FC12+gA		2		140
Triton X-100+gA		2		140
cyclohexane+gA		2		140
cholesterol+gA		2		140

Table S2. A summary of the derived $\Delta G_{gA-X}^{M\leftrightarrow D}$ values from the PMF decomposition analysis. Unit is kcal/mol.

$DC_{18:1}PC$ with	$\Delta G_{gA-bilayer}^{M\leftrightarrow D}$	$\Delta G_{gA-gA}^{M\leftrightarrow D}$	$\Delta G_{gA-drug}^{M\leftrightarrow D}$	$\Delta G_{gA-solvent}^{M\leftrightarrow D}$
bilayer only	4.1	-14.6	N/A	-1.6
capsaicin	2.6	-15.3	0.1	-1.1
resveratrol	3.2	-15.0	0.4	-1.5
octanol	2.6	-15.2	0.4	-0.9
C12E6	3.1	-15.1	-0.1	-0.6
FC12	1.3	-14.7	0.7	-0.2
Triton X-100	2.0	-14.4	-0.2	-0.2
cyclohexane	4.3	-14.9	-0.9	-1.1
cholesterol	4.7	-14.9	-1.4	-1.7
$DC_{22:1}PC$ with	$\Delta G_{gA-bilaye}^{M\leftrightarrow D}$	$\Delta G_{gA-gA}^{M\leftrightarrow D}$	$\Delta G_{gA-drug}^{M\leftrightarrow D}$	$\Delta G_{gA-solvent}^{M\leftrightarrow D}$
bilayer only	9.6	-15.6	N/A	-0.1
capsaicin	9.0	-15.7	0.1	0.7
resveratrol	8.9	-15.8	0.1	-0.2
octanol	7.7	-15.7	0.4	0.9
C12E6	6.7	-15.4	0.3	0.9
FC12	5.7	-15.6	1.0	1.0
Triton X-100	5.5	-15.6	0.3	0.9
cyclohexane	10.4	-15.3	-1.1	0.6
cholesterol	11.5	-15.5	-1.1	-0.1

Table S3. Drug partition coefficients into lipid bilayers

Drug	AlogP*	K_p
capsaicin	3.88	7.67×10^3
resveratrol	3.01	1.03×10^3
octanol	2.80	0.62×10^3
C12E6	3.83	6.84×10^3
FC12	3.04	1.10×10^3
Triton X-100	3.26	1.82×10^3
cyclohexane	2.74	0.55×10^3

*Estimated using the Schrödinger Suite (Schrödinger, New York, NY)

Table S4. Estimated $\Delta\Delta G^{M\leftrightarrow D}|_{Drug}$ at m_{Drug} = 0.084.

Drugs	gA		gD	
	$\Delta\Delta G^{M\leftrightarrow D}|_{Drug}$	r^2	$\Delta\Delta G^{M\leftrightarrow D}|_{Drug}$	r^2
capsaicin	-0.6	0.96	-0.5	0.94
resveratrol	-1.8	0.93	-1.7	0.72
octanol	-0.3	0.80	-0.4	0.73
C12E6	-1.5	0.42	-1.4	0.86
FC12	-0.5	1.00	-0.5	0.98
Triton X-100	-1.6	0.42	-1.5	0.75
cyclohexane	0.0	0.75	0.0	*N/A

*Approximation based on the nonlinear decrease of the number of channels in the presence of cyclohexane

SI References:

1. Durkin, J. T.; Providence, L. L.; Koeppe II, R. E.; Andersen, O. S., Formation of Non-Beta 6.3-Helical Gramicidin Channels between Sequence-Substituted Gramicidin Analogues. *Biophys. J.* **1992,** *62*, 145-159.

2. Durkin, J. T.; Providence, L. L.; Koeppe II, R. E.; Andersen, O. S., Energetics of Heterodimer Formation among Gramicidin Analogues with An NH2-terminal Addition or Deletion. Consequences of Missing A Residue at the Join in the Channel. *J. Mol. Biol.* **1993,** *231*, 1102-1121.

3. Marrink, S. J.; Risselada, H. J.; Yefimov, S.; Tieleman, D. P.; de Vries, A. H., The MARTINI Force Field: Coarse Grained Model for Biomolecular Simulations. *J. Phys. Chem. B* **2007,** *111*, 7812-7824.

4. Monticelli, L.; Kandasamy, S. K.; Periole, X.; Larson, R. G.; Tieleman, D. P.; Marrink, S. J., The MARTINI Coarse-Grained Force Field: Extension to Proteins. *J. Chem. Theory Comput.* **2008,** *4*, 819-834.

5. Sun, D. L.; Peyear, T. A.; Bennett, W. F. D.; Andersen, O. S.; Lightstone, F. C.; Ingólfsson, H. I., Molecular Mechanism for Gramicidin Dimerization and Dissociation in Bilayers of Different Thickness. *Biophys. J.* **2019,** *117*, 1831-1844.

6. Grunewald, F.; Rossi, G.; de Vries, A. H.; Marrink, S. J.; Monticelli, L., Transferable MARTINI Model of Poly(ethylene Oxide). *J. Phys. Chem. B* **2018**, 7436-7449.

7. Pizzirusso, A.; Nicola, A. D.; Milano, G., MARTINI Coarse-Grained Model of Triton TX-100 in Pure DPPC Monolayer and Bilayer Interfaces. *J. Phys. Chem. B* **2016**, 3821-3832.

8. Melo, M. N.; Ingólfsson, H. I.; Marrink, S. J., Parameters for Martini Sterols and Hopanoids Based on A Virtual-Site Description. *J. Chem. Phys.* **2015,** *143*, 243152.

9. Bussi, G.; Donadio, D.; Parrinello, M., Canonical sampling through velocity rescaling. *J. Chem. Phys.* **2007,** *126*, 014101.

10. Berendsen, H. J. C.; Postma, J. P. M.; van Gunsteren, W. F.; DiNola, A.; Haak, J. R., Molecular dynamics with coupling to An External Bath. *J. Chem. Phys.* **1984,** *81*, 3684-3690.

11. de Jong, D. H.; Baoukina, S.; Ingólfsson, H. I.; Marrink, S. J., Martini straight: boosting performance using a shorter cutoff and GPUs. *Comput. Phys. Commun.* **2016,** *199*, 1-7.

12. Allen, T. W.; Andersen, O. S.; Roux, B., Energetics of Ion Conduction through the Gramicidin Channel. *Proc. Natl. Acad. Sci. U. S. A.* **2004,** *101*, 117-122.

13. Roux, B.; Karplus, M., Ion Transport in A Model Gramicidin Channel. Structure and Thermodynamics. *Biophys. J.* **1991,** *59*, 961-981.

14. Trzesniak, D.; Kunz, A. P.; van Gunsteren, W. F., A Comparison of Methods to Compute the Potential of Mean Force. *ChemPhysChem* **2007,** *8*, 162-169.

15. Abraham, M. J.; Murtola, T.; Schulz, R.; Páll, S.; Smith, J. C.; Hess, B.; Lindahl, E., GROMACS: High Performance Molecular Simulations through Multi-Level Parallelism from Laptops to Supercomputers. *SoftwareX* **2015,** *1-2*, 19-25.

16. Hoover, W. G., Canonical Dynamics: Equilibrium Phase-Space Distributions. *Phys. Rev. A.* **1985,** *31*, 1695-1697.

17. Nosé, S., A Molecular Dynamics Method for Simulations in the Canonical Ensemble. *Mol. Phys.* **1984,** *52*, 255-268.

18. Parrinello, M.; Rahman, A., Polymorphic Transitions in Single Crystals: A New Molecular Dynamics Method. *J. Appl. Phys.* **1981,** *52*, 7182-7190.

19. Hess, B.; Bekker, H.; Berendsen, H. J. C., Lincs: A Linear Constraint Solver for Molecular Simulations. *J. Comput. Chem.* **1997,** *18*, 1463-1472.

20. Essmann, U.; Perera, L.; Berkowitz, M. L.; Darden, T.; Lee, H.; Pedersen, L. G., A Smooth Particle Mesh Ewald Method. *J. Chem. Phys.* **1995,** *103*, 8577-8593.

21. Ingólfsson, H. I.; Andersen, O. S., Screening for Small Molecules' Bilayer-Modifying Potential Using A Gramicidin-Based Fluorescence Assay. *Assay Drug Dev. Technol.* **2010,** *8*, 427-436.

22. Alejo, J. L.; Blanchard, S. C.; Andersen, O. S., Small-Molecule Photostabilizing Agents Are Modifiers of Lipid Bilayer Properties. *Biophys. J.* **2013,** *104*, 2410-2418.